Many-Body Gap Protection against Motional Dephasing of an Optical Clock Transition

Zhijing Niu,[1,*] Vera M. Schäfer,[1,2] Haoqing Zhang,[1,3] Cameron Wagner,[1] Nathan R. Taylor,[1] Dylan J. Young,[1] Eric Yilun Song,[1] Anjun Chu,[1,3] Ana Maria Rey,[1,3] and James K. Thompson[1,†]

[1]JILA, NIST, and Department of Physics, University of Colorado, Boulder, Colorado, USA
[2]Max-Planck-Institut für Kernphysik, Saupfercheckweg 1, 69117 Heidelberg, Germany
[3]Center for Theory of Quantum Matter, University of Colorado, Boulder, Colorado, USA

(Received 2 October 2024; revised 15 January 2025; accepted 7 February 2025; published 20 March 2025)

Quantum simulation and metrology with atoms, ions, and molecules often rely on using light fields to manipulate their internal states. The absorbed momentum from the light fields can induce spin-orbit coupling and associated motional-induced (Doppler) dephasing, which may limit the coherence time available for metrology and simulation. We experimentally demonstrate the suppression of Doppler dephasing on a strontium optical clock transition by enabling atomic interactions through a shared mode in a high-finesse optical ring cavity. The interactions create a many-body energy gap that increases with atom number, suppressing motional dephasing when it surpasses the dephasing energy scale. This collective approach offers an alternative to traditional methods, like Lamb-Dicke confinement or Mössbauer spectroscopy, for advancing optical quantum sensors and simulations.

DOI: 10.1103/PhysRevLett.134.113403

In many quantum simulation and metrology applications, it would be ideal to work in pristine conditions where the motional and internal degrees of freedom of atoms, ions, or molecules are totally decoupled from each other. For example, this scenario is particularly advantageous for atomic clocks or quantum magnetism exploration. However, when dealing with optical transitions, photons impart significant momentum when used to manipulate the internal state of the atoms. This so-called spin-orbit coupling, or coupling between motion and spin [1,2], can be a resource when under careful control, but it is just as often a drawback that leads to single particle dephasing that limits the precision and fidelity of both quantum metrology and simulation experiments.

Suppression of spin-orbit coupling or Doppler dephasing in fact has been a major driver of experimental efforts in the atomic physics community, leading to the development of laser-cooling techniques. Inspired by the pioneering work of Dicke [3] and Mössbauer [4,5], experiments now use strong trapping potentials to spatially localize the atoms to much less than the wavelength of light they absorb and emit, see Figs. 1(a)–1(c).

However, strong traps can introduce additional decoherence mechanisms. For instance, optical traps as used for neutral atoms can cause ac Stark shifts and light scattering [6], both of which must be controlled not only in quantum metrology, but also in state-of-the-art quantum computing and simulation settings with atoms, ions, and molecules. Also, new physics searches via precision spectroscopy [7] would benefit from relaxing the need for magic trapping. As such, it is extremely desirable to discover new and complementary ways to suppress motional dephasing.

In this work, we experimentally demonstrate a novel collective mechanism where an ensemble of strontium atoms interact via a shared optical mode of a ring cavity leading to the suppression of motional dephasing, see Figs. 1(b) and 1(d). The suppression arises from a self-generated many-body energy gap that creates an energy penalty for evolving to states of lower symmetry [8]. Such suppression was first observed recently in a Bragg matter-wave interferometer, where dressing lasers were used to generate cavity-mediated momentum-exchange interactions, extending the coherence time between atomic ground momentum states separated in energy by only ∼500 kHz [9]. Here we show that cavity-mediated exchange interactions can suppress Doppler dephasing for an optical clock transition with states separated by 400 THz [Fig. 1(f)], thus providing a new path for quantum sensing using optical transitions [7].

This new capability is part of the broader goal of understanding how to use many-body interactions to enhance quantum metrology and simulation. While the use of a many-body gap to prolong coherence between internal states has been explored in various settings including in standing wave optical cavities with strontium and rubidium atoms under tight confinement [10–12], Coulomb interacting ions [13], and atomic collisions [14–18], to our knowledge this is the first observation using an optical transition without single-particle Lamb-Dicke suppression of motional dephasing. This is achieved using a ring cavity with position-independent atom-cavity coupling, enabling genuine all-to-all

*Contact author: zhijing.niu@colorado.edu
†Contact author: jkt@jilau1.colorado.edu

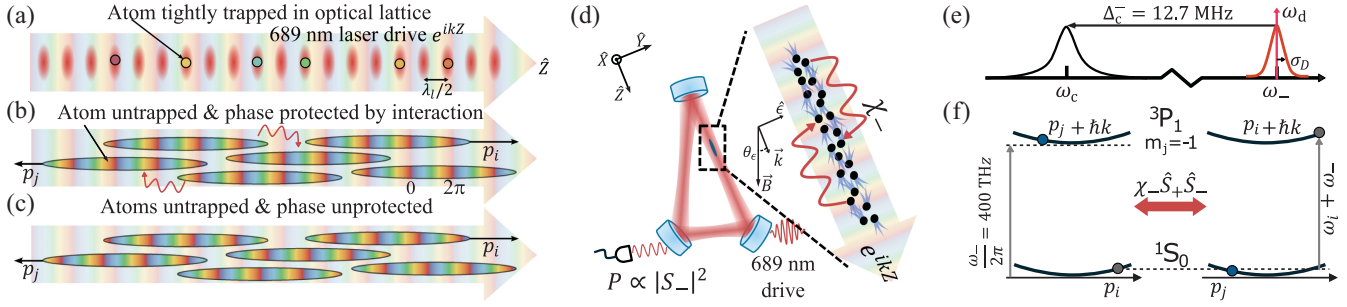

FIG. 1. Experimental setup. (a) Lamb-Dicke suppression of motional dephasing. An array of strontium atoms (dots) is tightly trapped in an optical lattice (red ovals) with wavelength λ_l and placed in a superposition of a ground $^1S_0$ and optically excited state $^3P_1, m_j = -1$ by a laser field along $\hat{Z}$ whose spatial phase e^{ikZ} is indicated via the color. Since the atoms are localized, the motional state is unchanged, and the superposition state of atom i at position Z_i simply acquires the local phase e^{ikZ_i} indicated by the color of the dot aligning to the spatial phase of the excitation laser. (b) If atoms are untrapped, we can model each atom as being a delocalized wave packet of approximately well-defined initial momenta p_i, p_j, etc. The laser excitation now imprints a spatially varying phase on the superposition of the ground and excited states. (c) Differences in kinetic energies cause the phases of different atoms to become randomized relative to each other and thus lead to a loss of collective coherence. Allowing the atoms to exchange photons [red squiggles in (b)] suppresses the motional dephasing. (d) The exchange of photons is mediated by a ring cavity. The laser drive at 689 nm excites the clockwise mode of the cavity with linear polarization $\hat{\epsilon}$ and mode function e^{ikZ}. A magnetic field $\vec{B}$ defines the quantization axis. We detect the optical power P from the clockwise mode after the laser excitation to measure the collective atomic coherence $|S_-|^2$ versus time. (e) The bare cavity ω_c is detuned by Δ_c^- from the atomic transition frequency ω_- that is inhomogeneously broadened by σ_D by the atomic motion (red). (f) Atoms can virtually exchange photons via the cavity, leading to an all-to-all effective spin-exchange interaction $\chi_- \hat{S}_+ \hat{S}_-$ in which atoms change both their internal and momentum states.

couplings without spatial inhomogeneities seen in previous implementations [10,12,15–18].

We also demonstrate a gap protection mechanism in a ring cavity beyond a two-level system by coupling to multiple optical excited states. The Hamiltonian of this extended system connects to models of modified neutrino oscillations in extreme astrophysical environments [19,20], relativistic quantum mechanical systems via spin-orbital coupling [21], or condensed matter systems featuring a Dirac cone dispersion such as graphene [22,23], and topological insulators [24,25] in a regime where interactions dominate, with easily tunable parameters of the simulated Hamiltonians.

In our experiment, $N = 10^6$ ^{88}Sr atoms are laser cooled and trapped in a high-finesse optical ring cavity using a 1D optical lattice at $\lambda_l = 813$ nm, and with radial temperature of 10 μK [Fig. 1(d) and [26]]. The lattice serves to position the atoms within the cavity mode but will be switched off during subsequent experiments so that atoms can freely move inside the cavity mode and experience Doppler dephasing.

The cavity's resonance frequency ω_c is red-detuned from the $\gamma = 2\pi \times 7.5$ kHz linewidth transition $^3P_1$-$^1S_0$ at frequency ω_0 by $\Delta_c^0 = \omega_c - \omega_0 = -2\pi \times 14$ MHz. The three-mirror cavity has a mode waist size of approximately 83 μm, finesse $\mathcal{F} = 6.2 \times 10^3$, and full-width-half-maximum (FWHM) linewidth is $\kappa = 2\pi \times 266$ kHz at the transition wavelength of $\lambda = 689$ nm for the relevant p-polarization mode $\hat{\epsilon}$ lying in the plane of the ring cavity. The magnetic field points downwards. The cavity wave vector $\vec{k}$ and cavity polarization $\hat{\epsilon}$ are at an angle $\theta_\epsilon = 20°$ from vertical and horizontal respectively [Fig. 1(d)]. The magnetic field sets the quantization axis and induces Zeeman splittings between adjacent excited states $|^3P_1, m_j\rangle$ levels by $\delta_B = 2\pi \times 1.3$ MHz. Under this field, we define detunings of the cavity relative to each atomic transition frequency $\Delta_c^{-,0,+} = \omega_c - (\omega_0 + m_j \delta_B)$ with $m_j = -1, 0, +1$. By orienting the $\vec{B}$ field in this way we manage to engineer a system where all three transitions between ground and excited m_j levels have nonzero coupling to the relevant cavity mode. The couplings give rise to single-photon Rabi frequencies $2g_0 = 2g \sin\theta_\epsilon$ and $2g_\pm = 2g \cos\theta_\epsilon/\sqrt{2}$ for $m_j = 0, \pm 1$ respectively. Here $g = 2\pi \times 3.5$ kHz.

For simplicity, we will consider the ith atom as initially being in the ground state $|\downarrow_i\rangle \equiv |g, p_i\rangle$ with initial momentum p_i along the cavity axis. The values of the p_i reflect the finite temperature of the atoms and are drawn from a 1D Gaussian distribution with zero mean and rms momentum spread σ_p. To determine σ_p, we perform time-of-flight expansion measurements after turning off the trapping lattice [27]. We find that the rms velocity spread along the cavity axis is $\sigma_v = 59(6)$ mm/s corresponding to a temperature of 38(8) μK.

We first consider the case in which we use a laser at frequency ω_d that is resonant with $m_j = -1$ atomic transition frequency ω_- to resonantly excite this transition by driving the clockwise cavity mode, with e^{ikZ} mode function [Fig. 1(d)]. The drive is sufficiently large to establish an intracavity Rabi frequency Ω_d to nominally place each atom in a superposition of ground and excited states irrespective of initial momentum p_i. The state after

the nominal $\pi/2$ pulse is $|\psi_{0,i}\rangle = (1/\sqrt{2})(|\downarrow_i\rangle + |\uparrow_i\rangle)$, but with the excited state portion of the wave function $|\uparrow_i\rangle \equiv |e, p_i + \hbar k\rangle$ now displaced by the momentum of the absorbed photon $\hbar k$ due to the spin-orbit coupling [1,2] during the excitation. Here $\hbar$ is the reduced Planck constant and $k = 2\pi/\lambda$, see Fig. 1(f). This translates to the position space as imprinting a phase factor e^{ikZ} on the atomic distribution.

We can describe the i th atom in terms of unitless single-particle pseudospin raising $\hat{s}_i^+ = |\uparrow_i\rangle\langle\downarrow_i|$ and lowering $\hat{s}_i^- = (\hat{s}_i^+)^\dagger$ operators, along with pseudospin projection operators $\hat{s}_i^z = \frac{1}{2}(|\uparrow_i\rangle\langle\uparrow_i| - |\downarrow_i\rangle\langle\downarrow_i|)$, $\hat{s}_i^x = \frac{1}{2}(\hat{s}_i^+ + \hat{s}_i^-)$ and $\hat{s}_i^y = (-i/2)(\hat{s}_i^+ - \hat{s}_i^-)$. Finally we define collective operators $\hat{S}_\alpha = \sum_{i=1}^N \hat{s}_i^\alpha$ with $\alpha \in \{x, y, z, +, -\}$. In the following, we will denote the expectation value of an operator with $A \equiv \langle\hat{A}\rangle$.

The coupling of the atoms to the cavity is described by the Tavis-Cummings Hamiltonian in the rotating frame of the atomic transition frequency ω_- as $\hat{H}_{\mathrm{TC}} = \hbar g_-(\hat{S}_+\hat{a} + \hat{S}_-\hat{a}^\dagger) + \hbar\Delta_c^-\hat{a}^\dagger\hat{a}$. The creation and annihilation operators $\hat{a}^\dagger$ and $\hat{a}$ describe the cavity mode that propagates in the same direction in which the initial atomic drive is applied. The counterclockwise mode is neglected since the collective coupling to this mode is proportional to the expectation value of the collective operator $(1/N)\langle\sum_{i=1}^N |\downarrow_i\rangle\langle e, p_i - \hbar k|\rangle$, which is zero for the initially prepared state and does not deviate from zero significantly due to collective or superradiant decay on the timescale of the experiment. The orthogonal s-polarized mode is detuned by 600 MHz due to mirror birefringence and thus can be safely neglected as well.

As experimentally demonstrated in [10,28], in the large detuning limit $|\Delta_c^-| \gg \sqrt{N}2g_-$ [29], the cavity mode can be adiabatically eliminated from the Tavis-Cummings Hamiltonian and one arrives at a cavity-mediated all-to-all spin-exchange Hamiltonian

$$\hat{H} = \hbar\chi_-\hat{S}_+\hat{S}_- + \hbar\sum_{i=1}^N \omega_i\hat{s}_i^z. \tag{1}$$

The exchange interaction strength is set by the frequency $\chi_- = ({g_-}^2/\Delta_c^-)/(1 + (\kappa/(2\Delta_c^-))^2) \approx g_-^2/\Delta_c^-$ for the large detuning we work at $|2\Delta_c^-/\kappa| > 100$.

The last term of Eq. (1) captures Doppler broadening [30] with $\hbar\omega_i$ simply the kinetic energy difference between the ground and excited state portions of the wave function that is not common to all atoms $\hbar\omega_i = \hbar k p_i/m$, where m is the mass of the atom. The distribution of ω_i inherits the properties of the initial rms spread in momentum σ_p such that the frequency distribution is described by a Gaussian distribution with zero mean and rms $\sigma_D = k\sigma_p/m \approx 2\pi \times 87(9)$ kHz. Ignoring interaction, single-particle Bloch vectors $\vec{s}_i = \{s_i^x, s_i^y, s_i^z\}$ precess at their own frequencies, shortening the total Bloch vector norm as a function of time with $|S_-(t)|^2 = |S_-(0)|^2 e^{-t^2/\tau_D^2}$ with $\tau_D = 1/\sigma_D = 1.8(2)$ μs, as illustrated in Fig. 2(b).

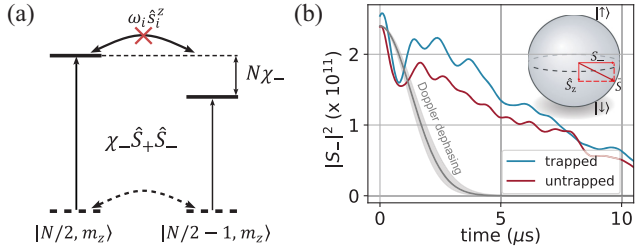

FIG. 2. Many-body gap protection of squared atomic coherence $|S_-|^2$. (a) The cavity-mediated collective exchange interaction opens an energy gap $N\chi_-$ between two initially degenerate states (dashed lines) $|S, m_z\rangle$ of total spin S and projection m_z. The many-body energy gap pushes the single-particle motional dephasing (modeled by single-particle terms $\omega_i\hat{s}_i^z$) off-resonance such that the total S remains constant and the atomic coherence is preserved. (b) The cavity field adiabatically follows atomic coherence S_- (see inset Bloch sphere) such that heterodyne detection of the weak leakage of field from the cavity allows us to determine $|S_-|^2$ versus time. After the 689 nm drive generates a $\pi/2$ pulse, Doppler dephasing would cause $|S_-|^2$ to decay rapidly as shown by the grey curve. The red curve is the experimentally observed coherence versus time when atoms are untrapped. The coherence extends well beyond the predicted Doppler dephasing based on time-of-flight measurement. The extension of coherence is achieved by operating at a collective interaction scale $N\chi_-/2\pi = 430(10)$ kHz. One also sees that the collective suppression of Doppler dephasing maintains coherence just as well as when one also imposes conventional single-particle trapping of the atoms in the Lamb-Dicke regime (blue curve).

The all-to-all exchange interaction can be approximated as $\hat{S}_+\hat{S}_- \approx \hat{\vec{S}}\cdot\hat{\vec{S}} - \hat{S}_z^2$. The first term means that there is an energy change associated with going to states of lower symmetry [Fig. 2(a)], with a characteristic energy gap $\hbar N\chi_-$ between adjacent states of total spin $S = N/2$ and $S = N/2 - 1$. This energy gap then competes with the single particle dephasing, protecting the spin alignment when $N\chi_- \gtrsim \sigma_D$ by essentially pushing the single particle motional dephasing off-resonance.

To observe suppression of Doppler dephasing, we load atoms into the intracavity optical lattice, switch off the cooling lasers and optical lattice, and wait 10.1 μs for lattice light to decay such that the atoms are no longer trapped. We note that radial expansion of the cloud and gravity can both be safely neglected for the approximate 40 μs duration of the full measurement sequence.

We then apply a nominal $\pi/2$ drive pulse on the $m_j = -1$ transition. The cavity field adiabatically follows the collective optical dipole moment $a \approx S_-(g/\Delta_c^-)$. As a result, we can infer S_- by detecting the very small amount of light that leaks from the cavity using heterodyne detection. We emphasize that $|S_-|/(N/2)$ indicates the contrast of

a hypothetical Ramsey fringe if measured after phase evolution time t. We average between 100 to 1200 repetitions of the experiment with more averaging for lower atom numbers.

In Fig. 2(b), the gray curve shows the predicted decay of $|S_-|^2$ for Doppler broadening as determined from the time-of-flight measurements without interaction. The red data curve shows that the measured coherence extends well beyond this timescale, directly indicating that Doppler dephasing is being suppressed by the interaction.

For comparison, we repeat the same experiment as above but leave the optical lattice on and tightly confine atoms in the traditional Lamb-Dicke regime suppressing Doppler dephasing via single-particle physics. The blue data curve of Fig. 2(b) for this case closely resembles the original Doppler-sensitive red data curve where, in contrast, the insensitivity arises from the collective interactions mediated by the cavity. Both curves decay more quickly than the excited state single-particle decay time of $\tau = 1/\gamma = 21$ μs, indicating that the excess decay primarily appears to arise from something other than Doppler dephasing.

For Doppler dephasing to be suppressed by the exchange interaction, the characteristic gap frequency should be larger than the dephasing frequency scale $N\chi_- > \sigma_D$. We observe this behavior in the data of Fig. 3, where we show the measured $|S_-|^2$ versus time for a range of $N\chi_-/2\pi$ from 130 to 430 kHz. We determine $N\chi_-$ by measuring dispersive shifts of the cavitylike mode at large N and then using this measurement to calibrate a fluorescence detection for smaller N [27]. The gap frequency is adjusted by varying the number of atoms at an earlier laser-cooling stage to avoid changing the temperature of the atomic ensemble. The minimum number of atom is limited by signal to noise in measuring $|S_-|^2$ since the detected signal scales as N^2.

For the smallest value of $N\chi_-/2\pi = 130(40)$ kHz, $|S_-|^2$ rapidly collapses with $1/e$ time 0.9(3) μs. However, as $N\chi_-$ increases slightly, the coherence begins to last substantially longer, with $|S_-|^2$ reaching a $1/e$ value at 10 μs at the largest value of $N\chi_-/2\pi = 430(10)$ kHz. When the frequency gap scale approaches the total dephasing frequency (see below) at $N\chi_-/2\pi = 170$ to 270 kHz, an oscillation with a frequency comparable to $\chi_- N$ emerges in $|S_-|^2$. This oscillation can be identified as a damped Higgs-like oscillation [9,12].

The observed decay of $|S_-|^2$ at $N\chi_-/2\pi = 130$ kHz is more rapid than that predicted for Doppler dephasing (gray curves). We believe that the Doppler dephasing prediction is accurate, and instead assign this to a magnetic field gradient across the atomic cloud that leads to a dephasing with rms frequency $\sigma_B = 2\pi \times 160(30)$ kHz. Exchange interaction also suppresses this dephasing as observed previously [12,31]. This excess dephasing also explains roughly half the difference in the coherences for the trapped and untrapped data in Fig. 2(b).

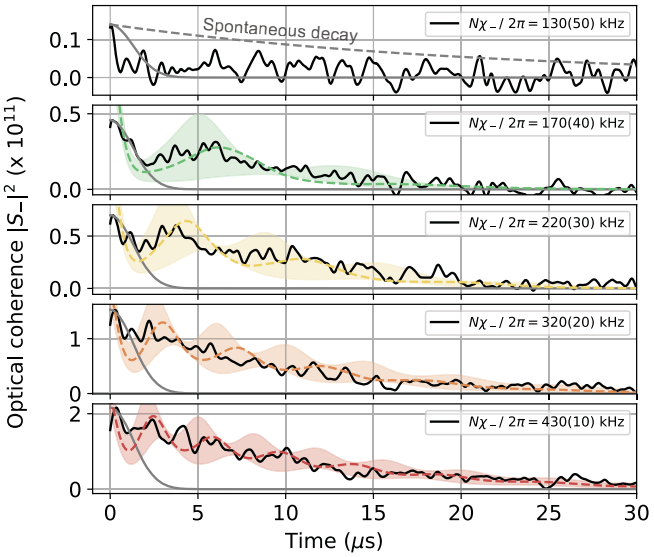

FIG. 3. Emergence of collective gap protection against Doppler dephasing by varying $N\chi_-$ via adjusting the number of atoms loaded into the cavity. With a small $N\chi_-$, coherence collapses more rapidly than the spontaneous decay (gray dashed curve), but increasing the atom number provides full protection against Doppler dephasing. Faster-than-expected coherence decay at small $N\chi_-$ is attributed to an additional spatial magnetic field inhomogeneity. The colored dashed curves are the numerical simulations using a mean-field simulation that includes interactions, dephasing, spontaneous decay, and collective decay. The colored bands indicate the range of the simulation variation for changes in N by ±10%.

The dashed numerical simulation curves in Fig. 3 agree relatively well with observations. The simulations use a mean-field master equation that includes the Hamiltonian dynamics of Eq. (1), single-particle spontaneous emission described by jump operators $\sqrt{\gamma/2}\hat{s}_i^-$, and collective decay described by a jump operator $\sqrt{\Gamma_s/2}\hat{S}_-$, with $\Gamma_s \approx \kappa(g_-/\Delta_c^-)^2$. For the simulations, the atom number N was adjusted upwards by 0%, 52%, 37%, 16%, −3%, respectively from top to bottom, to better describe each data set. We believe that this discrepancy may arise from an inaccuracy in the transfer of the calibration of $N\chi_-$ performed at the highest atom number but extended to lower atom number via fluourescence imaging of the atoms.

We can also observe gap protection against Doppler dephasing when we simultaneously excite $m_j = \pm 1$ [Fig. 4(a)]. In Fig. 4(b), we show the measured cavity output power versus time. We see rapid oscillations with an envelope persisting well beyond the timescale for single-particle Doppler dephasing. Exchange interactions lock each of the $m_j = \pm 1$ ensembles individually but not strongly enough to bind them together. This gives rise to beating in the output power at $2\delta_B$. We have seen similar oscillations in a standing wave cavity with trapped atoms, emulating phases of BCS superconductors [12,32]. Here,

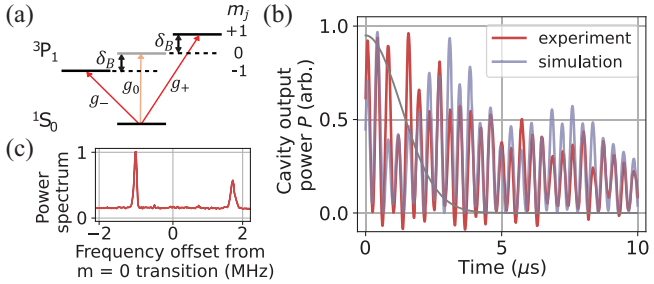

FIG. 4. Many-body gap protection and beating of the coherence with several excited states. (a) We simultaneously excite $m_j = \pm 1$ with Zeeman splitting δ_B by setting the drive to $\omega_d = \omega_0$ and increasing the drive's Rabi frequency. (b) The power emitted from the cavity, expressed as a total optical atomic coherence $|S_-|^2$ versus time shows beating at $2\delta_B$ [27], persisting well beyond the gray Doppler dephasing curve, demonstrating that the coherence on each transition is gap protected against Doppler dephasing. The gap for this data was set to $N\chi_-/2\pi = 430(10)$ kHz. (c) The power spectrum of detected light from $t = 0$ to 10 μs shows two discrete Fourier frequencies indicating that two Zeeman transitions independently radiate light.

both ensembles share the same ground state, and the oscillations are more pronounced and last longer due to the homogeneous cavity coupling. The power spectrum [Fig. 4(c)] shows light is being radiated largely independently from the two $m_j = \pm 1$ levels.

We have experimentally demonstrated that cavity-mediated interactions can suppress Doppler dephasing on a narrow optical clock transition at 400 THz. Beyond being of fundamental scientific interest, this provides a potentially new tool for optical metrology and spectroscopy [27], such as searches for new particles and fields through fast modulation of an optical atomic transition frequency [7]. The approach here also simultaneously enables measurements at timescales fast compared to the phase evolution time by detection of light emitted from the cavity.

In the future, exploring quantum simulation in this system with homogeneous atom-cavity coupling will also be of great interest, avoiding complications from inhomogeneous coupling in standing wave cavities. The two directionally independent cavity modes also provide a controllable degree of freedom that bears some similarity to tunable mode-changing collisions in quantum many-body systems. Additionally, connecting to models for neutrino-neutrino interactions, which lead to collective effects in flavor space [19], will be intriguing. By using three atomic levels to emulate three neutrino flavors, and both clockwise and counterclockwise cavity modes to controllably emulate trajectory-dependent interactions, we should be able to recreate simplified versions of such a model system.

Acknowledgments—This material is based upon work supported by the U.S. Department of Energy, Office of Science, National Quantum Information Science Research Centers, Quantum Systems Accelerator. We acknowledge additional funding support from the National Science Foundation under Grants No. 2317149 (Physics Frontier Center) and No. OMA-2016244 (Quantum Leap Challenge Institutes), the Vannevar Bush Faculty Fellowship, the Heising-Simons Foundation, and NIST. We acknowledge the valuable discussions with Chengyi Luo, Zhenpu Zhang, Shuo Sun and Joonseok Hur.

[1] Y. Lin, K. Jiménez-García, and I. B. Spielman, Nature (London) **471**, 83 (2011).
[2] S. Kolkowitz, S. Bromley, T. Bothwell, M. L. Wall, G. Marti, A. P. Koller, X. Zhang, A. M. Rey, and J. Ye, Nature (London) **542**, 66 (2017).
[3] R. H. Dicke, Phys. Rev. **89**, 472 (1953).
[4] R. L. Mössbauer, Z. Naturforsch. A **14**, 211 (1959).
[5] R. V. Pound and G. A. Rebka, Phys. Rev. Lett. **4**, 337 (1960).
[6] S. L. Campbell, R. B. Hutson, G. E. Marti, A. Goban, N. D. Oppong, R. L. McNally, L. Sonderhouse, J. M. Robinson, W. Zhang, B. J. Bloom, and J. Ye, Science **358**, 90 (2017).
[7] M. S. Safronova, D. Budker, D. DeMille, D. F. J. Kimball, A. Derevianko, and C. W. Clark, Rev. Mod. Phys. **90**, 025008 (2018).
[8] A. M. Rey, L. Jiang, M. Fleischhauer, E. Demler, and M. D. Lukin, Phys. Rev. A **77**, 052305 (2008).
[9] C. Luo, H. Zhang, V. P. W. Koh, J. D. Wilson, A. Chu, M. J. Holland, A. M. Rey, and J. K. Thompson, Science **384**, 551 (2024).
[10] M. A. Norcia, R. J. Lewis-Swan, J. R. Cline, B. Zhu, A. M. Rey, and J. K. Thompson, Science **361**, 259 (2018).
[11] E. J. Davis, A. Periwal, E. S. Cooper, G. Bentsen, S. J. Evered, K. Van Kirk, and M. H. Schleier-Smith, Phys. Rev. Lett. **125**, 060402 (2020).
[12] D. J. Young, A. Chu, E. Y. Song, D. Barberena, D. Wellnitz, Z. Niu, V. Schäfer, R. J. Lewis-Swan, A. M. Rey, and J. K. Thompson, Nature (London) **625**, 679 (2024).
[13] J. Franke, S. R. Muleady, R. Kaubruegger, F. Kranzl, R. Blatt, A. M. Rey, M. K. Joshi, and C. F. Roos, Nature (London) **621**, 740 (2023).
[14] J. C. Allred, R. N. Lyman, T. W. Kornack, and M. V. Romalis, Phys. Rev. Lett. **89**, 130801 (2002).
[15] C. Deutsch, F. Ramirez-Martinez, C. Lacroûte, F. Reinhard, T. Schneider, J. N. Fuchs, F. Piéchon, F. Laloë, J. Reichel, and P. Rosenbusch, Phys. Rev. Lett. **105**, 020401 (2010).
[16] S. Smale, P. He, B. A. Olsen, K. G. Jackson, H. Sharum, S. Trotzky, J. Marino, A. M. Rey, and J. H. Thywissen, Sci. Adv. **5**, eaax1568 (2019).
[17] J. Huang, C. A. Royse, I. Arakelyan, and J. E. Thomas, Phys. Rev. A **108**, L041304 (2023).
[18] J. Huang and J. E. Thomas, Phys. Rev. A **109**, L041301 (2024).
[19] A. B. Balantekin, M. J. Cervia, A. V. Patwardhan, E. Rrapaj, and P. Siwach, Eur. Phys. J. A **59**, 186 (2023).
[20] P. Siwach, A. M. Suliga, and A. B. Balantekin, Phys. Rev. D **107**, 023019 (2023).
[21] L. J. LeBlanc, M. C. Beeler, K. Jiménez-García, A. R. Perry, S. Sugawa, R. A. Williams, and I. B. Spielman, New J. Phys. **15**, 073011 (2013).
[22] K. S. Novoselov, Rev. Mod. Phys. **83**, 837 (2011).

[23] L. Huang, Z. Meng, P. Wang, P. Peng, S.-L. Zhang, L. Chen, D. Li, Q. Zhou, and J. Zhang, Nat. Phys. **12**, 540 (2016).
[24] M. Z. Hasan and C. L. Kane, Rev. Mod. Phys. **82**, 3045 (2010).
[25] N. Goldman, G. Juzeliūnas, P. Öhberg, and I. B. Spielman, Rep. Prog. Phys. **77**, 126401 (2014).
[26] J. R. K. Cline, V. M. Schäfer, Z. Niu, D. J. Young, T. H. Yoon, and J. K. Thompson, Phys. Rev. Lett. **134**, 013403 (2025).
[27] See Supplemental Material at http://link.aps.org/supplemental/10.1103/PhysRevLett.134.113403, which includes Ref. [26], for additional information about the experimental methods and a detailed discussion of the scaling of the gap protection.
[28] E. J. Davis, G. Bentsen, L. Homeier, T. Li, and M. H. Schleier-Smith, Phys. Rev. Lett. **122**, 010405 (2019).
[29] J. A. Muniz, D. Barberena, R. J. Lewis-Swan, D. J. Young, J. R. Cline, A. M. Rey, and J. K. Thompson, Nature (London) **580**, 602 (2020).
[30] A. Shankar, L. Salvi, M. L. Chiofalo, N. Poli, and M. J. Holland, Quantum Sci. Technol. **4**, 045010 (2019).
[31] S. Scherg, T. Kohlert, P. Sala, F. Pollmann, B. Hebbe Madhusudhana, I. Bloch, and M. Aidelsburger, Nat. Commun. **12**, 4490 (2021).
[32] D. J. Young, E. Y. Song, A. Chu, D. Barberena, Z. Niu, V. M. Schäfer, R. J. Lewis-Swan, A. M. Rey, and J. K. Thompson, arXiv:2408.12640.